JOURNAL OF MATERIALS SCIENCE 10 (1975) 1161–1168

Low-temperature deformation mechanisms in an Fe–Si–Ti alloy

D. H. JACK
Department of Metallurgy, Leeds University, Leeds, UK

F. GUIU
Department of Materials, Queen Mary College, University of London, London, UK

The temperature and strain-rate dependence of the yield and flow stresses of an age-hardened Fe–Si–Ti alloy, and a binary Fe–Si alloy, have been investigated in the temperature range 77 to 330 K. The parameters of activated deformation have been determined as a function of the precipitate dispersion and it is concluded that these parameters are unaffected by precipitation even when particles are sheared by dislocations, implying that bcc iron alloys cannot be dispersion strengthened at room temperature without making them even stronger, and hence more brittle, at lower temperatures. Work-hardening of all alloys is due to increases in the athermal component of the applied stress. The activation enthalpy at low effective stresses is larger than that for pure iron, indicating that silicon exerts a higher lattice friction stress due to its effect on the core asymmetry of screw dislocations in iron.

1. Introduction

Dilute alloys of iron with silicon and titanium exhibit a marked age-hardening response when solution-treated above 1000°C, quenched, and aged in the temperature range 500 to 750°C [1-3]. The hardening is due to homogeneous precipitation of finely dispersed spherical particles of a metastable phase which has been shown to have the ordered $L2_1$ crystal structure and a composition close to Fe_2TiSi [4]. The structure is an fcc superlattice of bcc iron, with both silicon and titanium in ordered sites, and the unit cell edge length is 1.995 times that of the matrix. Particles are observed to be coherent up to diameters of 1500 Å, and persist for long ageing times even though they are eventually replaced by the equilibrium Laves phase, Fe_2Ti.

The strengthening due to these particles has been discussed in a previous paper [5] and is consistent with a model in which the ordered particles are cut by single dislocations when the alloy is aged up to peak strength. Beyond peak strength the yield stress is close to that predicted by the Orowan mechanism and considerable by-passing of the particles by dislocation cross-slip is observed.

The present paper deals with the temperature and strain-rate dependence of the yield and flow stress of Fe–Si–Ti, both when particles are sheared by dislocations and when they are by-passed. The results are discussed in terms of the theory of thermally activated flow at low temperatures.

2. Experimental procedures

The alloys investigated, analyses for which are given in Table I, were prepared by arc-melting under a partial pressure of argon. A standard solution-treatment of 2 h at 1150°C was followed by water quenching. Ageing of the Fe–Si–Ti alloy was carried out at 600°C for times up to 125 h. A previous investigation [6] has established that under these ageing conditions, the volume fraction of precipitate is 6% and hence

TABLE I Analyses of alloys used

Alloy	Fe	Si	Ti	C	N	O
	wt %					
Fe–Si	97.2	2.8	<0.01	0.011	0.001	0.006
	at. %					
	94.6	5.4	—	—	—	—
Fe–Si–Ti	wt %					
	94.80	3.65	1.55	0.006	0.001	0.004
	at. %					
	91.27	6.99	1.74	—	—	—

the residual solute content of the matrix is 5.5 at. % Si and 0.25 at. % Ti. Thus the binary Fe–Si alloy has a composition close to that of the matrix of the age-hardened Fe–Si–Ti. At all stages of heat-treatment, each alloy is ferritic, with a grain size (mean intercept length) of 0.2 mm.

The extreme brittleness of precipitation-hardened Fe–Si–Ti alloys prevents deformation studies in tension if more than 1 % plastic strain is required. Compression tests were, therefore, carried out in an "Instron" testing machine model TT-CM-L at a basic strain-rate of 1.4×10^{-4} sec^{-1}. The compressive strain was imposed using a stainless steel jig which could be immersed in a cold liquid bath, containing a mixture of liquid nitrogen and "Isceon", for low-temperature tests.

Cylindrical specimens, 6 mm long and 2.3 mm diameter, were compressed between two tungsten carbide inserts. The specimens were obtained from a swaged bar which had been given a standard solution-treatment. Rods about 50 mm long were machined to 2.4 mm diameter, electropolished, and cut by spark machining to 8 mm lengths. They were finally ground by hand to 6 mm lengths with parallel ends. These specimens were annealed for 15 min at the solution-treatment temperature, quenched, and aged appropriately. Changes in temperature and strain-rate were made during deformation and the associated load increments were measured from the flow stress curve extrapolated onto the elastic line.

The absence of a well-defined yield stress, and the different work-hardening rates of alloys containing different precipitate dispersions, make it necessary to establish a criterion for comparing experimental yield stresses with those predicted from theoretical models. Etch-pit experiments were, therefore, performed in order to assess the significance of various points on the load-extension curves of strip specimens tested in tension. The initial carbon content of the alloys is too low to produce etch pits, so after straining, the strips were carburized before electro-etching. At stresses below the proportional limit, etch pits are only observed close to grain boundaries and are not aligned into slip bands. At and beyond the proportional limit, dislocation sources have operated and, in suitably oriented grains, narrow slip bands traverse the grains. For these alloys, the proportional limit was, therefore, taken as the appropriate stress to compare with the theoretical models, and in calculating shear stresses, τ, from tensile stress, σ, a Schmid factor, $\tau/\sigma = 0.5$ was used.

3. Experimental results

3.1. Stress-strain behaviour

Typical true stress-strain curves at different temperatures for variously heat-treated Fe–Si–Ti alloys, and for the Fe–Si alloy are shown in Fig. 1. Only the binary Fe–Si alloy exhibits a yield point, indicating that its absence in Fe–Si–Ti is probably due to the removal of interstitial solute by titanium. Additional solid-solution strengthening by the extra 1.5 at. % each of silicon and titanium is considered responsible for the increase in yield stress in going from binary Fe–Si to as-quenched Fe–Si–Ti.

Fig. 2 shows the variation of shear yield stress with ageing time and mean particle radius. Thus an ageing treatment of 1 h at 600°C produces a dispersion of particles with a mean radius of 25 Å and centre-to-centre separation of 150 Å, at which stage the alloy has reached peak strength. After 125 h ageing at 600°C, the mean particle radius is 115 Å and the separation is 700 Å. The higher work-hardening rate of the overaged alloy (see Fig. 1) reflects the change from a particle cutting mechanism to a by-passing mechanism beyond peak strength.

The apparently high *initial* work-hardening rate of alloys aged to peak strength is due to the fact that at this stage dislocations are straight and confined to their slip planes, implying that cross-slip, and hence dislocation multiplication, are more difficult. If multiplication by cross-slip is inhibited, and sufficient sources are not available, the imposed strain-rate must be matched by increasing the velocity of the available mobile dislocations, i.e. increasing the stress. Hence the apparently high initial work-hardening rate is a consequence of the time taken to establish a mobile dislocation density sufficient to match the imposed strain-rate.

3.2. Temperature dependence of the yield and flow stress

The variation with temperature of the proportional limit, the lower yield point or 0.2 % proof stress and the stress at 8 % strain is shown in Fig. 3a to d for Fe–Si and variously treated Fe–Si–Ti. The discontinuity at about 250 K in the curves for binary Fe–Si has also been observed previously by other workers [7].

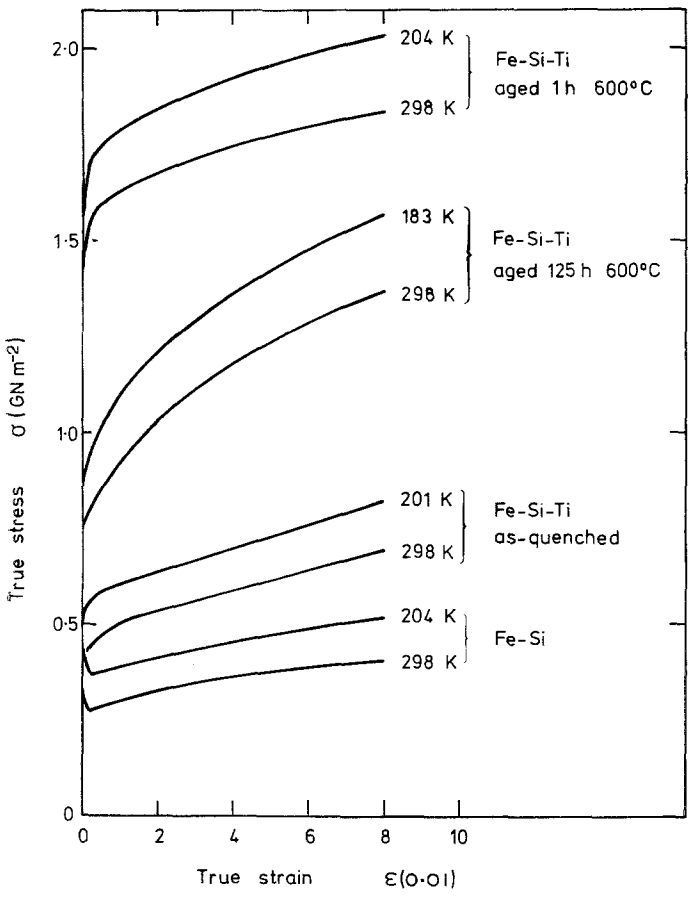

Figure 1 Compressive true stress-true plastic strain curves for Fe–Si and Fe–Si–Ti variously heat-treated.

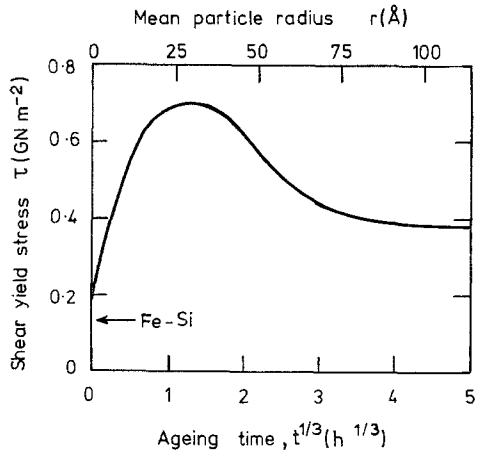

Figure 2 Variation of shear yield stress, $\tau = \sigma/2$, with ageing time for Fe–Si–Ti.

The applied stress, σ, can be regarded as the sum of the two terms:

$$\sigma = \sigma^*(T) + \sigma_\mu$$

where $\sigma^*(T)$ and σ_μ are the effective stress required to assist thermal activation and the athermal stress, respectively. In order to find an approximate value for the temperature T_c at which $\sigma^*(T)$ becomes negligible, the slopes $d\sigma/dT$ of the curves of Fig. 3 are plotted against temperature as a solid line in Fig. 4a and b. Neglecting the variation of σ_μ with temperature (due to changes in the elastic modulus), the transition between thermally activated and athermal regions (where $d\sigma/dT = 0$) is found to occur at 435 ± 20 K for the Fe–Si alloy and 460 ± 30 K for the Fe–Si–Ti alloy, regardless of heat-treatment. Even if the variation of the elastic modulus with temperature is taken into account, see Conrad and Hayes [8], it would only reduce T_c by ~ 10 K, within the limits of error of the estimated T_c. Confirmation of the values obtained comes from the work of Granas and Aronsson [7] who have measured the temperature dependence of the 0.2% proof stress of

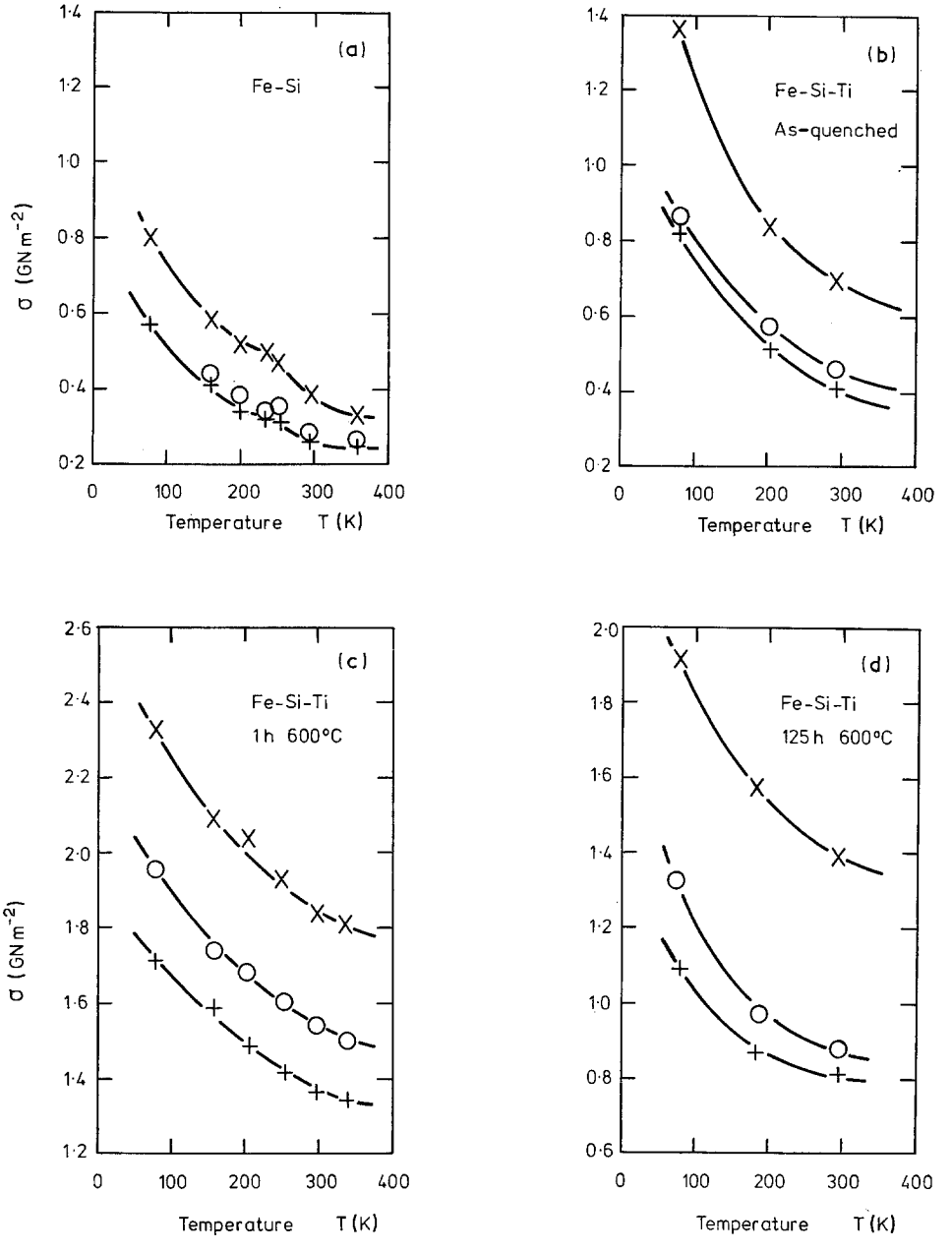

Figure 3 Variations of compressive proportional limit (+); 0.2% proof stress (○); and flow stress at 8% true plastic strain (×) for: (a) Fe–Si; (b) Fe–Si–Ti, as-quenched; (c) Fe–Si–Ti, aged 1 h 600°C; (d) Fe–Si–Ti aged 125 h 600°C.

various Fe–Si alloys up to 800 K. They find that T_c increases with silicon content, with $T_c \simeq 530$ K for Fe–5% Si and $\simeq 590$ K for Fe–7% Si.

As well as measuring the temperature dependence of the proportional limit, temperature changes of about 15 K were made at approximately 4% strain in a series of tests with different initial temperatures. These values $\Delta\sigma/\Delta T$ are superimposed on the continuous plots of Fig. 4, and show that to all intents the temperature

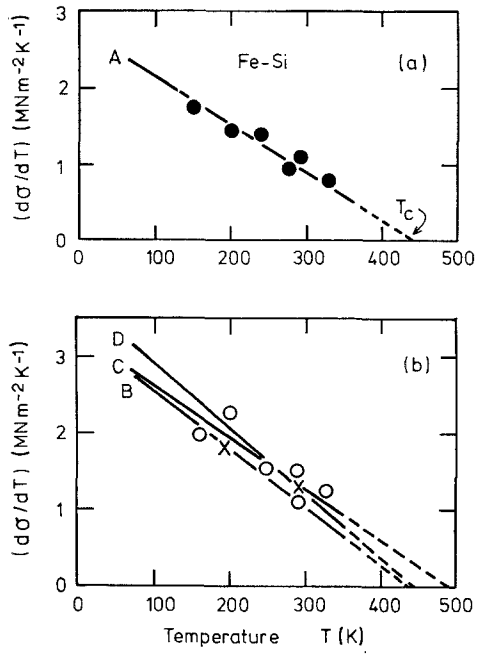

Figure 4 (a) and (b) Variation of temperature dependence of the yield stress for: Fe–Si (line A); Fe–Si–Ti, as-quenched (line B); Fe–Si–Ti, aged 1 h 600°C (line C); Fe–Si–Ti aged 125 h 600°C (line D). Superimposed upon the continuous lines are points obtained from temperature change experiments at approximately 4% plastic strain in Fe–Si (●); Fe–Si–Ti as-quenched (×); Fe–Si–Ti, aged 1 h 600°C (○).

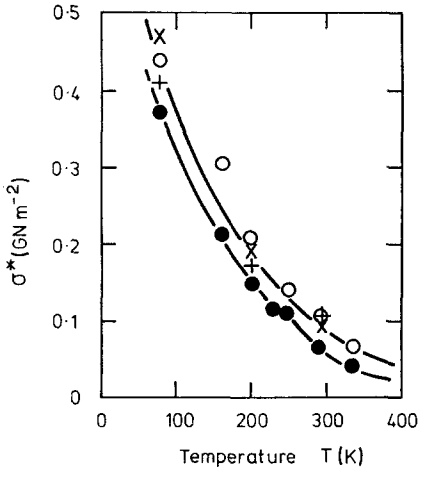

Figure 5 Variation of the effective compressive stress, σ^*, with temperature for: Fe–Si (●); Fe–Si–Ti, as quenched (×); Fe–Si–Ti, aged 1 h 600°C (○); Fe–Si–Ti aged 125 h 600°C (+).

dependence of the flow stress at this strain is the same as that of the proportional limit.

Values of σ_μ at T_c were obtained in the present work from the extrapolation of plots of σ versus $1/T$, which approximate to straight lines at high temperatures. These values are found to be 0.21 ± 0.02 GN m^{-2}; 0.31 ± 0.02 GN m^{-2}; 1.26 ± 0.02 GN m^{-2} and 0.67 ± 0.02 GN m^{-2} for the Fe–Si and the Fe–Ti–Si alloy as-quenched, aged for 1 h and aged for 125 h at 600°C, respectively. It is thus possible to plot the variation of σ^* with temperature for the various heat-treated alloys, as in Fig. 5. It is obvious that σ^* and its temperature dependence are both independent of the heat-treatment of the alloy and hence of precipitate size. At a given temperature, the effective stress for the Fe–Si–Ti is slightly greater than that for the binary Fe–Si, which is a result of the different values of T_c chosen for the two alloys, but the difference falls within the limits of error in the values of σ_μ obtained from the estimates of T_c.

3.3. Strain-rate dependence of the stress

The changes in applied stress, $\Delta\sigma$, associated with a ten-fold change in strain-rate were plotted as a function of strain for the different alloys. The $\Delta\sigma$, for an increase in strain-rate, was found to be approximately equal to the $\Delta\sigma$ for a decrease, at all strains. The plots of $\Delta\sigma$ against strain are published elsewhere [9], but here only the values of $\Delta\sigma$ extrapolated to zero strain are given in Table II.

4. Discussion

4.1. Thermally activated deformation

The thermally activated strain-rate, $\dot{\epsilon}$, is usually described by a rate equation of the form

$$\dot{\epsilon} = \dot{\epsilon}_0 \exp(-\Delta H/kT) \qquad (1)$$

where $\dot{\epsilon}_0$ is a frequency factor containing both the entropy term and a geometrical factor which converts compressive strain, ϵ, into shear strain and thus makes the equation applicable to polycrystalline samples. ΔH is the enthalpy of activation for forward dislocation movement if this overcomes a single type of obstacle, and k is Boltzmann's constant. The activation enthalpy can be obtained for the temperature and strain-rate dependence of the shear yield stress:

$$\Delta H = -TA^*\boldsymbol{b}\left(\frac{\partial\tau^*}{\partial T}\right)_{\dot{\epsilon}/\epsilon_0} \qquad (2)$$

where the activation area A^* is given by:

TABLE II Compressive stress changes, $\Delta\sigma$, for a 10:1 change in strain-rate, extrapolated to zero strain

Fe–Si		Fe–Si–Ti					
		As-quenched		1 h 600°C		125 h 600°C	
$\Delta\sigma$ (MN m^{-2})	T (K)	$\Delta\sigma$ (MN m^{-2})	T (K)	$\Delta\sigma$ (MN m^{-2})	T (K)	$\Delta\sigma$ (MN m^{-2})	T (K)
17.7	77	22.5	77	25.2	77	26.5	77
19.4	160	—	—	25.9	163	—	—
13.0	200	21.0	201	25.1	204	21.7	183
15.2	235	—	—	—	—	—	—
16.6	251	—	—	19.8	251	—	—
11.5	296	16.0	298	16.1	298	16.2	296
9.0	334	—	—	16.4	336	—	—

$$A^* = \frac{-kT}{b}\left[\frac{\partial \ln(\dot{\epsilon}/\epsilon_0)}{\partial \tau^*}\right]_T. \qquad (3)$$

The activation parameters can, therefore, be calculated using the results of temperature and strain-rate change experiments, and the influence of precipitate particles on the deformation parameters can thus be ascertained.

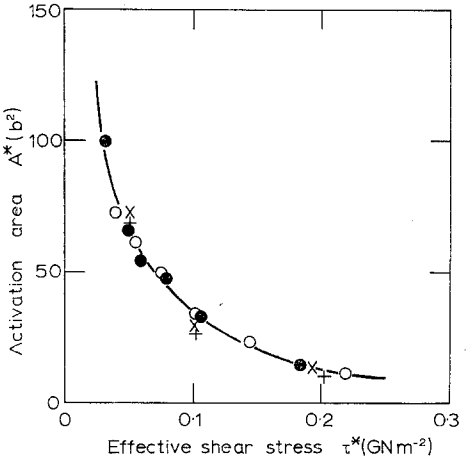

Figure 6 Variation of activation area, A^*, with effective shear stress, τ^*, for: Fe–Si (●); Fe–Si–Ti, as-quenched (×); Fe–Si–Ti, aged 1 h 600°C (○); Fe–Si–Ti aged 125 h 600°C (+).

The activation area A^* was calculated using Equation 3 and the data of Table II for the various alloys and heat-treatments. The values obtained are plotted atainst the effective shear stress, $\tau^* = \sigma^*/2$, in Fig. 6. The activation enthalpies obtained using Equation 2 and the data of Fig. 4, are plotted against effective stress in Fig. 7. It is apparent from the results of Figs. 6 and 7 that the observed values of A^* and ΔH are the same, at the same effective stress, for Fe–5.5 at % Si and for Fe–7 at % Si–1.75 at. % Ti solution-treated, aged 1 h at 600°C and aged 125 h at 600°C. By implication, the activated process responsible for these values is also the same and is most probably that of overcoming the intrinsic lattice friction, or Peierls stress, which is known to be large in substitutional bcc alloys and in particular in Fe–Si [10].

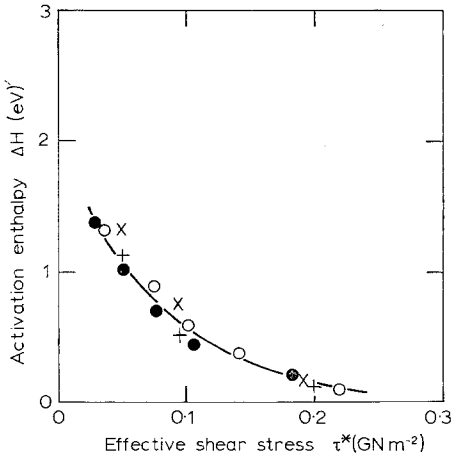

Figure 7 Variation of activation enthalpy, $\triangle H$, with effective shear stress, τ^*, for: Fe–Si (●); Fe–Si–Ti, as-quenched (×); Fe–Si–Ti, aged 1 h 600°C (○); Fe–Si–Ti aged 125 h 600°C (+).

The values of ΔH extrapolated to zero stress are about twice as large as those of other workers for pure iron [11, 12]. This extrapolation must be treated cautiously, however, since Equation 1 is only valid when $A^* b \tau^* \gg kT$ and loses its validity as τ^* approaches zero [13].

However, ΔH for Fe–Si and Fe–Si–Ti is consistently higher at any stress than that for pure iron, and this is assumed to indicate the operation at low temperatures of a Peierls mechanism with a higher lattice friction. The addition of silicon is believed to increase the magnitude of the core asymmetry of screw dislocations in iron and hence reduce their mobility.

Whatever the activated process responsible for the observed values of A^* and ΔH, it is apparent that throughout the temperature range investigated it is the same, at the same effective stress, no matter what the precipitate dispersion in Fe–Si–Ti.

In the overaged alloy, when the Orowan mechanism is operating, precipitates may not be expected to alter the activation parameters, but where dislocations shear small, closely spaced, particles, a change in the temperature dependence of the effective stress may have been expected. It seems, however, that the precipitate particles in the Fe–Si matrix act somewhat like point defects in a matrix with a strong lattice friction [14]. In this case, the temperature dependence of the effective stress of the matrix is so strong that precipitates, even when they are sheared, contribute only by increasing the athermal component of the stress. This is an important result because it implies that bcc iron alloys cannot be disperson strengthened at room temperature without making them even stronger, and hence more brittle, at lower temperatures.

Papaleo and Whiteman [15] have also examined the temperature dependence of the flow stress in a similar Fe–Si–Ti alloy, but conclude that the activation parameters do vary with heat-treatment. Their results relate to the high-temperature range 200 to 400 K, where the deformation mechanisms are more difficult to identify, and where the effective stress is most sensitive to a choice of T_c. It is suggested that the experimental errors in determining T_c are responsible for the discrepancies between the two results.

4.2. Variation of effective stress with strain

The plastic strain-rate is also often described by an empirical equation of the form

$$\dot{\gamma} = B(\tau^*)^{m^*}$$

where B and m^* are constants that depend on temperature. The exponent m^* is calculated from the strain-rate dependence of σ^* at zero strain using the approximation:

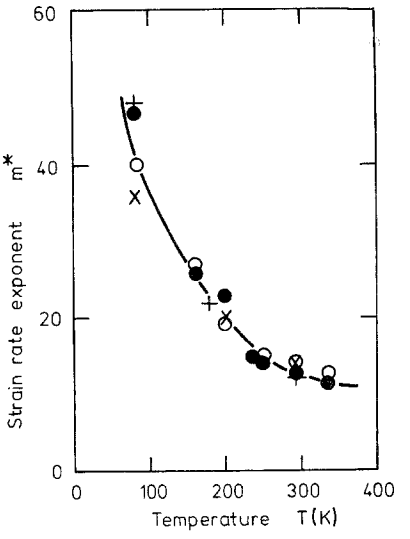

Figure 8 Variation of strain-rate exponent, m^*, with temperature for: Fe–Si (●); Fe–Si–Ti, as quenched (×); Fe–Si–Ti, aged 1 h 600°C (○); Fe–Si–Ti aged 125 h 600°C (+).

$$m^* = \tau^* \Delta \ln \dot{\gamma} / \Delta \tau^* = \sigma^* \Delta \ln \dot{\epsilon} / \Delta \sigma^* . \quad (4)$$

The values of m^* thus calculated at different temperatures and alloy heat-treatments are shown in Fig. 8. These values of m^* are in good agreement with those obtained from strain-rate changes in Fe–Si [7], but are lower than those obtained by direct measurements of dislocation velocity as a function of applied stress. It has been proposed [16] that the reason for such discrepancies is that in the etch-pit experiments, the motion of edge-dislocations is observed, whereas the macroscopic flow stress is controlled by the motion of screws. A further possible reason is that in the etch-pit experiments the measured stress is the applied stress, not the effective stress.

Again it is observed that m^* and its temperature dependence are the same for Fe–Si and Fe–Si–Ti with different precipitate dispersions. If it is assumed that m^* is a constant of the material independent of strain, the change of σ^* with strain can be calculated from the observed variations of $\Delta \ln \dot{\epsilon} / \Delta \sigma^*$ with strain and using Equation 4 [17, 18]. When this was done it was found that in all cases σ^* remains practically constant with strain, see Fig. 9, which explains why the temperature dependence of the applied stress is observed to be independent of strain. It also suggests that the work-hardening is,

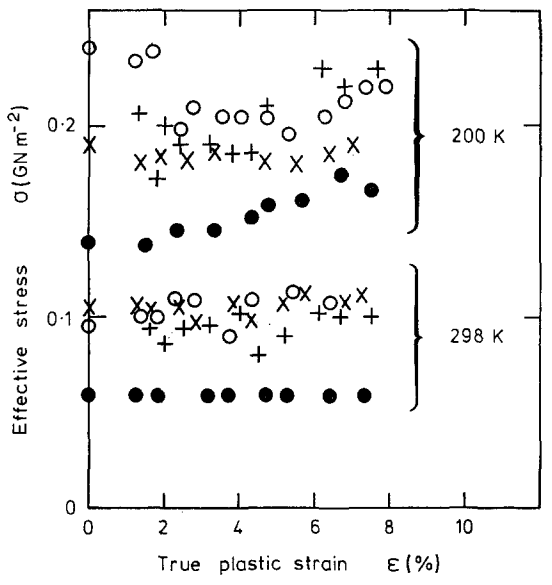

Figure 9 Variation of effective compressive stress, σ^*, with strain at approximately 298 and 200 K for: Fe–Si (●); Fe–Si–Ti, as-quenched (×); Fe–Si–Ti aged 1 h 600°C (○); Fe–Si–Ti, aged 125 h 600°C (+).

therefore, due almost exclusively to an increase in the internal stress caused by the elastic interaction of dislocations, and not to changes in the mobile dislocation density.

5. Conclusions

The temperature and strain-rate dependence of the yield and flow stress and by implication the rate-controlling deformation mechanisms of Fe–Si–Ti alloys are unaffected by the presence of particles even if these are sheared by dislocations. This, in turn, implies that precipitation hardening of bcc iron will result in even greater hardnesses, and hence brittleness, at low temperatures. The values of the activation enthalpy at low effective stresses are larger than those quoted for pure iron, due to the increased lattice friction stress in the presence of silicon.

The work-hardening of the variously heat-treated alloys is due to an increase in the athermal component of the applied stress.

Acknowledgements

The experimental portions of this investigation were carried out in the Department of Metallurgy, University of Cambridge and the authors would wish to thank Professor Honeycombe for his encouragement during the course of the work, and for the provision of laboratory facilities.

References

1. R. WASMUHT, *Arch. Eisenhüttenw.* **5** (1931) 45.
2. J. P. HENON, C. WACHE and J. MANENC, *Mem. Sci. Rev. Met.* **63** (1966) 99.
3. D. J. ABSON, G. G. BROWN and J. A. WHITEMAN, *J. Austr. Inst. Metals* **13** (1968) 61.
4. D. H. JACK, *Met. Sci. J.* **4** (1970) 22.
5. D. H. JACK and F. GUIU, "Proceedings of the 2nd International Conference on Strength of Metals and Alloys" (A.S.M., Cleveland, Ohio, 1970) p. 606.
6. D. H. JACK and R. W. K. HONEYCOMBE, *Acta Met.* **20** (1972) 787.
7. L. GRÅNÄS and B. AARONSON, *Scripta Met.* **2** (1968) 541.
8. H. CONRAD and W. HAYES, *Trans. ASM* **56** (1963) 125.
9. D. H. JACK, Ph.D. Thesis, University of Cambridge (1969).
10. J. W. CHRISTIAN, Proceedings of the 2nd International Conference on Strength of Metals and Alloys (A.S.M., Cleveland, Ohio, 1970) p. 31.
11. H. CONRAD and S. FREDERICK, *Acta Met.* **10** (1962) 1013.
12. J. W. CHRISTIAN and B. C. MASTERS, *Proc. Roy. Soc.* **A281** (1964) 223, 240.
13. G. ALEFELD, *Z. Naturforsch.* **17a** (1962) 889.
14. F. GUIU, *Phil. Mag.* **20** (1969) 51.
15. R. PAPALEO and J. A. WHITEMAN, "Effect of 2nd Phase Particles on the Mechanical Properties of Steel" (I.S.I., London, 1970) p. 22.
16. R. J. ARSENAULT, *Scripta Met.* **3** (1969) 419.
17. J. T. MICHALAK, *Acta Met.* **13** (1965) 213.
18. F. GUIU, *Phys. Stat. Sol.* **19** (1967) 339.

Received 22 November 1974 and accepted 8 January 1975.